Scanning Tunneling Microscopy Imaging of Small Adsorbed Molecules on Metal Surfaces in an Ultrahigh Vacuum Environment

Shirley Chiang*

Department of Physics, University of California, Davis, California 95616

Received March 31, 1997 (Revised Manuscript Received April 16, 1997)

Contents

Shirley Chiang received her A.B. degree *summa cum laude* (1976) in physics from Harvard University, and her M.A. (1978) and Ph.D. (1983) degrees in physics from the University of California, Berkeley. She was a Research Staff Member at the IBM Almaden Research Center from 1983–1994. In 1994, she joined the faculty of the Department of Physics at the University of California, Davis, as a Professor. She was named a Fellow of the American Physical Society in 1994. Dr. Chiang's current research interests center on using ultrahigh vacuum scanning tunneling microscopy (STM), atomic force microscopy (AFM), and low-energy electron microscopy (LEEM) for atomic resolution imaging of small molecules on metals and structural studies of heteroepitaxial metal-on-metal systems. Her earlier STM work included studies of reconstructed semiconductor and metal surfaces, atomic and molecular adsorbates, and deposition of nanometer-size islands. She has also previously used AFM for studying atomic-scale frictional forces. Dr. Chiang is currently the Chair of the Nanometer-scale Science and Technology Division of the American Vacuum Society and a member of the Executive Committee of the Materials Science Division of the American Physical Society.

I. Introduction

The development of the scanning tunneling microscope (STM) by Binnig and Rohrer[1] was extremely important because, for the first time, it enabled the imaging of solid surfaces with atomic resolution. Early applications of the STM concentrated on imaging of clean semiconductor and metal surfaces, with elucidation of both the physical and electronic structure of many systems. Early STM images of molecules, however, were not promising because they did not yield high resolution. For example, although the reconstruction of Pt(100) induced by chemisorbed CO molecules was observed, the individual CO molecules were not resolved.[2,3] Low-resolution images were also obtained for copper phthalocyanine molecules on silver films and were attributed to the effect of the applied electric field of the tunneling tip on the surface diffusion of the molecules.[4] Images of a cadmium arachidate bilayer on graphite, deposited by the Langmuir−Blodgett technique, showed bright elliptical spots in STM constant height images, which were assigned to individual molecules which were diffusing rapidly in the field of view.[5] In addition, STM images of the products of the chemical reaction of ammonia dissociating on the Si(111) (7×7) show that the contrast of dangling bond states of the Si changes upon reaction with ammonia.[6]

Within a few years, however, the STM was successfully applied to the imaging of individual molecules on surfaces. To date, many different types of molecules have been successfully imaged by STM,[7] including conducting organic molecular crystals (e.g., TTF−TCNQ),[8] liquid crystals,[9−12] polymers,[13−16] fullerenes,[17−25] and biological molecules.[26] Atomic scale resolution has been obtained on many molecule−substrate systems. For certain chemisorbed systems, the STM molecular images are of extremely high resolution, showing internal structure of the molecules with details that can be often understood by comparison with the calculated density of states of the molecule−substrate system. Such images may be used to determine molecular adsorption sites on surfaces. In addition, high-resolution STM images have recently been used to investigate the details of chemical reactions on surfaces, such as site specificity and reaction kinetics. These applications of molecular imaging will continue to grow in importance in the future. This review concentrates on the imaging of small adsorbed molecules on metal surfaces in an ultrahigh vacuum (UHV) environment, as these are systems for which particularly high molecular resolution images have been obtained.

* Author to whom correspondence should be addressed. Fax: 916-752-4717. E-mail: chiang@physics.ucdavis.edu.

S0009-2665(94)00555-8 CCC: $28.00

A number of factors which influence how well the STM can image a particular molecule on a given surface have been discussed in detail in several recent publications.[27−30] A key factor is the contribution of the adsorbate electronic structure to the STM image. If the STM image is dominated by the adsorbate electronic states, the molecular image can be more readily interpreted than if the STM image is dominated by the electronic structure of the substrate with a small modification induced by the adsorbed species. Thus, STM imaging of adsorbed molecules has been successful when the adsorbate contribution to the wave function is >10%, while imaging of the internal structure of adsorbed molecules has been most successful for strongly chemisorbed molecules for which the adsorbate contribution to the wave function is ∼30−50%.[27] Characteristics of the substrate, such as flatness and cleanliness, can also affect how easily adsorbed molecular structures can be distinguished from substrate structures.[28]

Characteristics of the tip, such as its size and geometry, as well as its chemical composition,[31] can affect the images. The tip can exert significant forces on the molecules, both van der Waals and electrostatic ones,[29,30] which can cause molecular motion during imaging. Of course, such motion can be used to deliberately place atoms on a surface in a particular arrangement.[32,33] Choosing a voltage and a current which move the tip closer to the surface may result in higher resolution images, if there are appropriate molecular electronic states for tunneling, but may also induce motion of the molecule. The amount of molecular diffusion or rotation on the surface during imaging may determine whether high-resolution imaging is possible.[34] Parameters such as temperature, coverage, and coadsorption[35] of other molecules can be varied to adjust the diffusion constant of an adsorbed molecule on the surface. Adsorption in different binding sites can change the observed molecular images because the electronic structure of the adsorbate−substrate system varies for different sites.[36] The symmetry of the molecule with respect to the substrate affects the reproducibility of binding sites and therefore how easily a particular structure in an image may be associated with an adsorbed molecule.[37] In addition, the STM images always involve both topographic and electronic contributions, which can be difficult to separate.

The mechanisms for transfer of the tunneling current between the tip and sample and for molecular contrast in STM imaging are not completely understood, and numerous possible explanations have been discussed. One proposed contrast mechanism is that the variations in the polarizability of the molecule could cause a spatially varying work function, leading to molecular contrast in STM images.[38] Another possibility considers electronic states in organic molecules which evolve by relaxation processes after injection of a charge, assuming a strong dependence on the interaction between the tip and sample for the charge injection.[39] Other mechanisms are the intramolecular through-bond charge transfer process[40] and nonresonant through-bond or through-space tunneling processes.[41] Surface conductivity has also been discussed as an explanation for measuring tunneling currents on insulating molecular layers.[42]

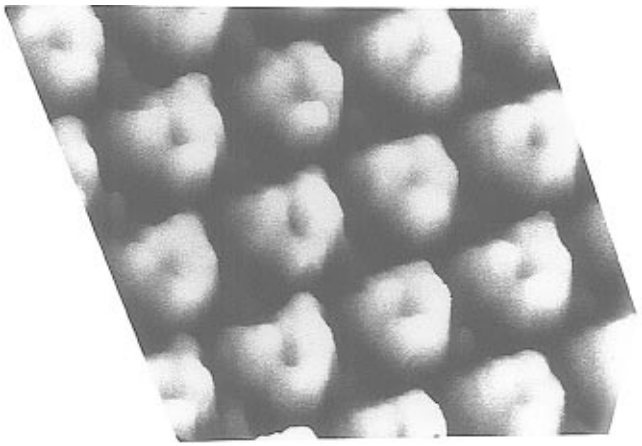

Figure 1. Three dimensional view of STM image of benzene coadsorbed with CO in (3×3) structure on Rh(111). Benzene molecules appear 3-fold, ∼2 Å high, with a depression at the center: $V_t = -0.01$ V, $I_t = 2$ nA. (Reprinted from ref 43. Copyright 1988 American Institute of Physics.)

Successful high-resolution STM images of small adsorbed molecules on single-crystal metal surfaces in a UHV environment have now been obtained on many systems. Those discussed below fall into the following categories: (a) small aromatic molecules, including particularly benzene, naphthalene, and azulenes, (b) porphyrins, particularly copper phthalocyanine, (c) carbon monoxide, (d) ethylene, and (e) other molecules.

II. Aromatic Molecules

a. Benzene

Benzene was the first molecule to be successfully imaged on a surface by high-resolution STM. Ohtani et al.[43] coadsorbed benzene and CO together on Rh(111) in a (3×3)(C_6H_6+2CO) structure and obtained the first high-resolution images showing that benzene has a ring structure (Figure 1). The structure of this surface had previously been determined by dynamical low-energy electron diffraction (LEED) analysis.[44] The unit cell has one benzene molecule lying flat and two upright CO molecules, all chemisorbed over hcp-type 3-fold hollow sites directly above second-layer Rh atoms. Note that the benzene molecule appears to have 3-fold symmetry because the STM images molecular orbitals which are hybridized with the rhodium substrate atoms below; the lobes of the observed benzene features are situated over the bridge sites between two rhodium atoms. The CO molecules in the unit cell, however, were not clearly resolved in the (3×3) structure. Subsequent measurements of the c(2√3×4) rectangular structure on Rh(111), which has one benzene molecule and one CO molecule per unit cell, did resolve CO molecules for the first time.[45] These results first demonstrated that the STM could be used to distinguish two different types of molecules on a surface, with great implications for the real space imaging of chemical reactions on surfaces. Images of this latter overlayer also showed features such as translational and rotational domain boundaries, molecules adsorbed near step edges, and evidence for surface diffusion.[46]

A very recent study of coadsorbed benzene and CO on Rh(111) used STM imaging to study the dynamics of ordering as a function of CO coverage.[47] The time evolution of the surface structures was observed, both for CO introduced onto a benzene-covered surface and for benzene introduced onto a CO-covered surface. Benzene was found to adsorb preferentially at steps at low coverage where it is immobile and therefore easily imaged by STM. CO inhibited the diffusion of benzene on the surface and helped to form ordered overlayers.

Weiss and Eigler immobilized benzene on Pt(111) for STM imaging by using an instrument at 4 K.[48] The STM images of the isolated benzene molecules had three different characteristic shapes: (1) a three-lobed structure, observed in two rotational orientations, 60° apart, similar to that previously observed for benzene on Rh(111),[43] (2) a cylindrical volcano with a small depression in the center, and (3) a simple bump (Figure 2). These different types of images were ascribed to different adsorption sites on the surface by comparing with the calculated images of Sautet and Bocquet.[36] Those calculations used the electron-scattering quantum chemistry (ESQC) technique of Sautet and Joachim to calculate the tunneling current between the tip and substrate through a molecule from the generalized Landauer formula using a scattering matrix, which has been calculated exactly.[49,50] The electronic structures of the tip, molecule, and substrate were calculated using extended Hückel molecular orbital theory. The calculated images were used to assign the three-lobed structures to benzene in both hcp-type and fcc-type 3-fold hollow adsorption sites, while the volcano structure and the simple bump were assigned to an on-top site and a bridge site respectively. Clearly, through their sensitivity to the detailed surface electronic structure, the STM images can be used to provide information on the chemical environment of a molecule. This same dependence, however, can complicate the identification of different molecules in an STM image.

Benzene molecules have also been observed on Cu(111) at 77 K.[51,52] This system was used as a model of a two-dimensional gas−solid interface. The STM permitted the imaging of the interface between adsorbed benzene forming a two-dimensional (2D) solid structure along the Cu step edges and benzene molecules on terraces which move freely across the surface as a 2D molecular gas. The atomic scale dynamics of this interface was studied by imaging the motion of individual molecules near the Cu(111) step edges. Lateral diffusion, 2D adsorption, and 2D desorption were observed at the interface between the 2D gas and the 2D solid.

Benzene in a c(4×2) structure on Pd(110) was imaged under tunneling conditions that allowed resolution of both the benzene features and the Pd surface atomic corrugation, allowing the determination of a 4-fold hollow binding site of the surface.[53] STM imaging was performed over the temperature range from 100 to 300 K, and the benzene molecules were observed to migrate on the surface above ∼220 K. From the images as a function of temperature, the migration barrier along the [001] direction was estimated at about 0.57 eV.

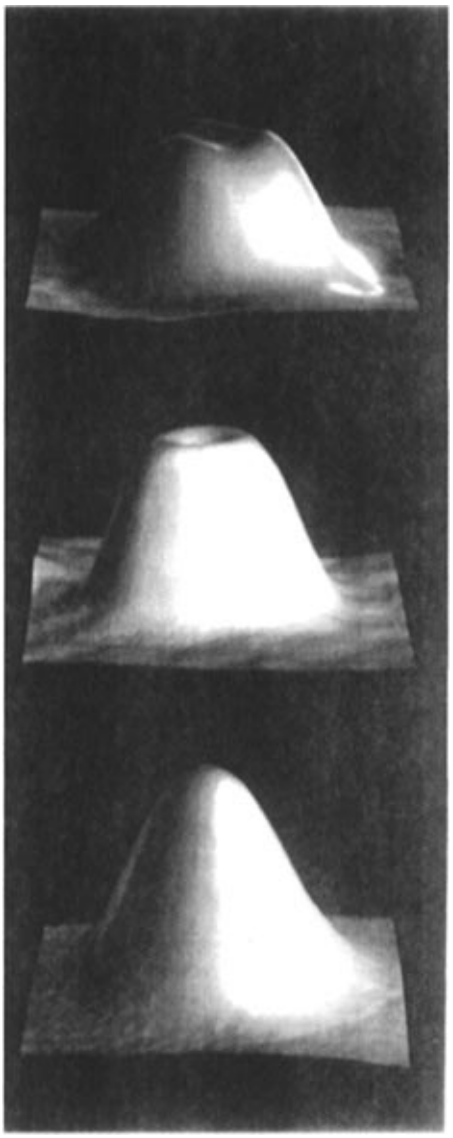

Figure 2. STM image of three different 15 Å × 15 Å regions, each showing a single adsorbed benzene molecule. These images have been assigned to (a, top) hcp 3-fold hollow site, (b, middle) on top site, and (c, bottom) bridge site, respectively. The images were recorded with (a) $V_{bias} = -0.050$ V, $I_t = 100$ pA; (b) $V_{bias} = -0.010$ V, $I_t = 1$ nA; (c) $V_{bias} = -0.010$ V, $I_t = 100$ pA. The minimum to maximum height differences in the images are (a) 0.58 Å, (b) 0.72 Å, and (c) 0.91 Å, respectively. The observed images of the individual molecules did not change qualitatively for a wide range of tunneling parameters. (Reprinted from ref 48. Copyright 1993 American Institute of Physics.)

Benzene has also been observed to interact with an oxygen-precovered Ni(110) surface at room temperature.[54] For an initial oxygen coverage of 0.3 monolayer (ML), the benzene causes a compression of the Ni−O added rows from a (3×1) to a (2×1) structure, and the benzene molecules occupy the troughs created by the compression. The benzene molecules disappeared from the images due to the dissociation of the molecules as the temperature was raised above ∼400 K.

Strohmaier et al.[55] measured very high-resolution images of hexabromobenzene (C_6Br_6) on highly oriented pyrolytic graphite (HOPG) and on MoS_2. The flat-lying molecules form a close-packed, incommensurate, physisorbed array on these substrates at

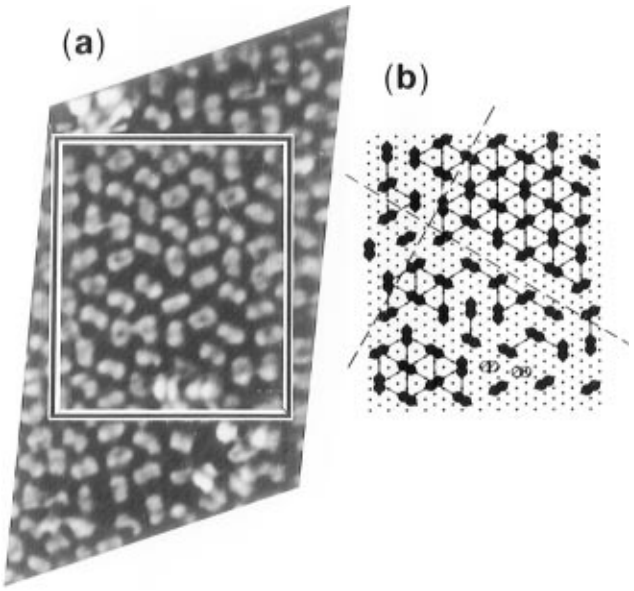

Figure 3. (a) High-resolution STM image of ordered naphthalene on Pt(111), ~90 Å × 150 Å in size, V_{sample} = +0.822 V, I_t = 2.5 nA. Naphthalene corrugation is ~1 Å high. The image skewing is due to the correction for severe thermal drift at the time of the data collection. (b) Schematic diagram of the overlap of a Pt(111) lattice with molecular positions. Glide symmetries are indicated by dashed lines. (Reprinted from ref 57. Copyright 1991 American Institute of Physics.)

room temperature. In images with submolecular resolution, the molecules appear different on the two substrates, although the molecular image contrast does not depend on the adsorption site for these substrates. The detailed submolecular pattern depends strongly on the tunneling voltage for molecules adsorbed on graphite. On MoS_2, the molecules show a less-pronounced inner structure, as expected from calculations for benzene on this substrate by Fisher and Blöchl.[56]

b. Naphthalene, Azulene, and Methylazulenes on Pt(111)

Hallmark, et al. performed a series of high-resolution STM studies on naphthalene ($C_{10}H_8$), azulene ($C_{10}H_8$), and several methylazulenes on Pt(111).[34,35,57−62] These molecules are strongly chemisorbed on Pt(111), making room temperature STM imaging possible. Naphthalene on Pt(111) forms an ordered (6×3) structure on Pt(111) when the molecule is deposited onto a substrate at temperatures between 100 and 200 °C. This structure has a LEED pattern with missing beams ascribed to glide plane symmetries.[63] Figure 3 shows an STM image of this structure, in which the molecules appear as bilobed structures, with three rotational orientations on the surface, 120° apart.[57] The molecules are situated on (3×3) Pt lattice sites in small domains, typically <50 Å apart. Domain boundaries usually involve a molecular shift by an additional Pt lattice constant, as shown in the schematic diagram in Figure 3b. Despite the fact that very few of the proposed (6×3) herringbone unit cells are seen, the molecular arrangement does possess a high degree of order:

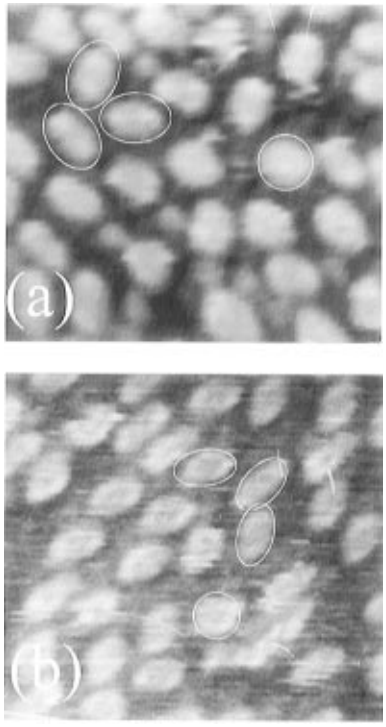

Figure 4. Coadsorbed naphthalene and azulene on Pt(111) with all three orientations of the elongated naphthalene molecules marked with ovals and symmetric azulene molecules marked by circles (~90 Å × 90 Å, V_t = −0.05 V, I_t = 1 nA). Typical molecular height is ~1 Å. (a) Low-resolution image. (b) Higher resolution, with double rings apparent for naphthalene and single rings for azulene. (Reprinted from ref 35. Copyright 1993 Elsevier.)

~40% of the molecules in the (3×3) domains satisfy the required glide plane symmetry operations and ~30% of the molecules display correlated orientations at six times the Pt lattice spacing. The bright defect spots in the image probably correspond to neighboring tilted molecules located closer to one another than to the Pt (3×3) lattice sites. Images were also measured for low-coverage naphthalene, for which subsequent images showed evidence for rotating and translating molecules, and for disordered naphthalene adsorbed at room temperature.[58]

Azulene ($C_{10}H_8$) has a 7-membered ring and a 5-membered ring and is an isomer of naphthalene. When adsorbed at low coverage on Pt(111), the STM has difficulty measuring individual molecules as they diffuse rapidly on the surface at room temperature.[35] At near saturation coverage, however, discrete azulene molecules are imaged as round bumps. Coadsorption of naphthalene and azulene together on Pt(111) leads to two advantages for STM imaging: (1) the more strongly bonded naphthalene helps to localize azulene molecules on the surface so that they can be better imaged and (2) examining both types of molecules simultaneously with the same tip eliminates tip artifacts from affecting the comparison of the images of the two types of molecules with one another.[35,60] In images of the coadsorbed isomers, naphthalene typically appears as a bilobed feature, while azulene typically appears as a single bump (Figure 4a). Very occasionally, with a particularly good tip, naphthalene appears as a double ring and azulene appears as single ring (Figure 4b).

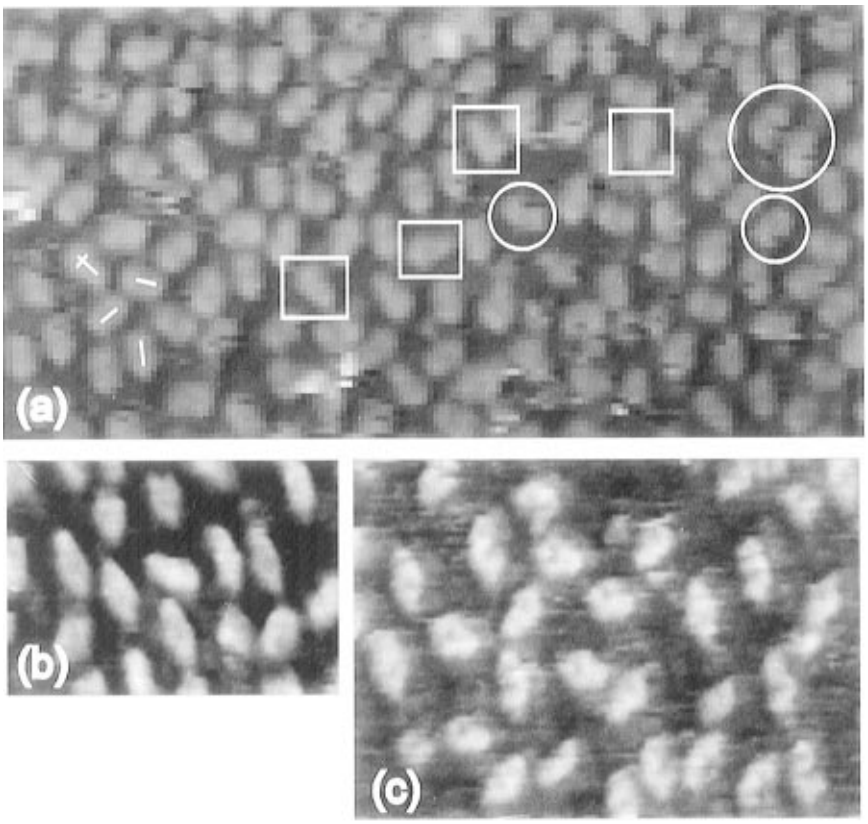

Figure 5. (a) Sample with coadsorbed 1-methylazulene (e.g., in circles) and 2-methylazulene (2-MA) (e.g., in squares) and then saturated with naphthalene. Long bars in left corner show three possible orientations of naphthalene molecules. The long axis of the pear-shaped 2-MA molecule, indicated by cross, is oriented 30° from the naphthalene axis. Typical molecular height is ~1 Å. (b) Low-resolution image of 6-methylazulene (6-MA), showing diamond shapes. (c) High-resolution image of 6-MA, showing internal molecular structure. (Reprinted from ref 34. Copyright 1994 American Vacuum Society.)

Three different isomers of monomethylazulene have also been adsorbed onto Pt(111) and imaged by the STM.[34,35,61] The images can be used to distinguish 1-methylazulene (kidney-bean shape) and 2-methylazulene (pear shape) when they are coadsorbed together on the surface (Figure 5a). Low-resolution images of 6-methylazulene display a diamond shape (Figure 5b), while high-resolution images of this molecule display internal structure (Figure 5c). Dimethylazulene and trimethylazulene can also be individually imaged by the STM, with trimethylazulene appearing as a 4-fold cloverleaf with one bright spot and dimethylazulene appearing quite similar.[34,61] The STM images were clearly useful for distinguishing these related molecules (naphthalene, azulene, and various methylazulenes) on the Pt(111) surface on the basis of their observed shapes. Comparing STM images also allows for determination of the relative sticking coefficients and relative diffusion rates for this series of molecules at room temperature.[34] The orientations and binding sites of several of these molecules on the surface could also be assigned. In addition, extended Hückel molecular orbital calculations for an individual adsorbed molecule on a cluster of Pt atoms were used to calculate the expected local density of states at the Fermi level for the molecule−substrate system, thus giving predicted STM images.[61,62] These predicted images appear to agree quite well with the measured images for this series of molecules, with the exception of azulene which moves too quickly at room temperature.

c. Other Aromatic Molecules

Many other aromatic molecules have now been imaged with molecular resolution on metal surfaces. These include thiophenes, phenoxy species, and pyrimidine.

STM images of thiophene, 2,5-dimethylthiophene, and 2,2′-bithiophene on Ag(111) have been obtained at 120 K.[64,65] All three molecules were found to preferentially adsorb at step edges. While thiophene molecules appeared nearly circular, the 2,5-dimethylthiophene, and 2,2′-bithiophene appear to be elongated at the step edge, reflecting the intrinsic shapes of these molecules. Figure 6 shows STM images of three different ordered structures of thiophene on Ag(111) as a function of increasing coverage. The higher coverage structures have higher packing density, suggesting that the thiophene molecules in Figure 6c and possibly also in Figure 6b are tilted away from the surface and interacting with it through the sulfur lone pair orbitals. Thiophene occupies the upper step edge at lowest coverage and, in addition, the lower step edge at higher coverage. The STM images give direct evidence for the preferential rotational alignment of molecules adsorbed at step edges. The 2,2′-bithiophene has the long molecular axis aligned parallel to the step edges. In contrast, the 2,5-dimethylthiophene adsorbs with the molecule aligned perpendicular to the step edge. Clustering of these molecules near the step edge suggests that the interaction between molecules at the step edge is attractive.

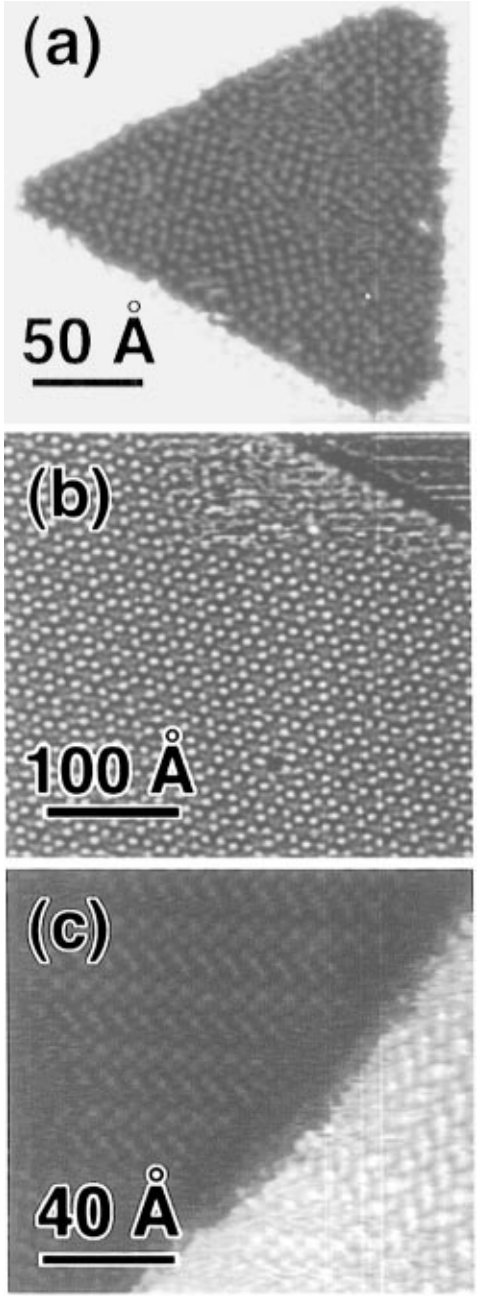

Figure 6. STM images of Ag(111) exposed to thiophene at increasing coverage. (a) A 40 L exposure, producing c(2√3×4) rect ordered overlayer, with three domains evident in the image. (b) A 90 L exposure, producing (2√7×2√7) overlayer. (c) A 150 L exposure, producing herringbone structure. (Reprinted from ref 65. Copyright 1996 American Vacuum Society.)

The order and periodicity of 3-thiophenecarboxylic acid on Cu(110) in the c(4×8) and p(2×1) structures have also been investigated in a study using high-resolution electron energy loss spectroscopy (HREELS), STM, and LEED.[66] The size and spacing of the bright features in the STM images for the c(4×8) structure with coverage of 0.25 ML suggest that the each feature is a single upright thiophene carboxylate species. At higher coverage (∼0.5 ML), the more densely packed p(2×1) structure has molecules with the rings twisting out of plane, as inferred from HREELS.

STM has also been used to investigate the monolayer structure of adsorbed phenoxy (PhO) species on Cu(110), which is formed by exposing the surface to phenol (PhOH) at room temperature.[67] Individual molecules are clearly observed in the images, and the ordering of the molecules is examined. Although a c(4×2) LEED pattern was found, three different overlayer structures for the adsorbed molecules were observed: (1) a densely packed c(4×2) or $\begin{pmatrix} 4 & 0 \\ 0 & 2 \end{pmatrix}$ structure with a coverage of 0.25 PhO per surface copper atom (Figure 7), (2) more densely packed phenoxy chains separating the c(4×2) regions with a local coverage of 0.33PhO per Cu, and (3) a distorted c(4×2) or $\begin{pmatrix} 4 & 0 \\ 1 & 2 \end{pmatrix}$ structure consisting of phenoxy chains. The dimensions of the structures in the STM images were used to develop structural models, which have a constant binding site for the phenoxy species and different orientations (from nearly parallel to almost normal) with respect to the surface plane.

Isolated molecules of pyrimidine (1,3-diazine, $C_4H_4N_2$) on Pd(110) are observed in STM images as 0.6 nm × 0.6 nm rectangular shapes with two parts of elongated protrusions.[68] Two binding sites are observed: on the row and between the [1$\bar{1}$0] close-packed rows of the Pd(110) surface. Even at low coverage, 20−30% of the molecules form dimers, indicating a strong attractive interaction between two adsorbed molecules.

Monolayers of the organic molecules naphthalene-1,4,5,8-tetracarboxylic dianhydride (NTCDA)[69] and perylene-3,4,9,10-tetracarboxylic dianhydride (PTCDA)[70] have also been studied on graphite and on MoS_2, both weakly interacting substrates. Internal structure was observed for these molecules and was correlated with the calculated molecular electronic structure. Various crystallographic phases of these materials, including both flat-lying molecules on the surface and bulklike stacks of molecules with the molecular plane perpendicular to the substrate, were also observed.

III. Porphyrins

a. Copper Phthalocyanine

Lippel et al. obtained the first STM images showing the internal structure of isolated molecules for the system of copper phthalocyanine (Cu-phth) on Cu(100).[37] The STM images show molecules adsorbed in two different rotational orientations, in agreement with the two different domains evident in LEED measurements.[71] For the first time, unusual molecular binding sites at step edges were observed, an important step toward studying the chemical reactivity of such sites. Figure 8 shows high-resolution images of this molecule, with the internal structure clearly evident. The observed internal structures compare well with the calculated highest occupied molecular orbital (HOMO) of the free molecule which was embedded in the experimental image. Tip-induced motion was observed, as was an isolated molecule above a measurably corrugated metal surface. For this system, the choice of substrate allowed the molecule to adsorb in a unique binding site, thus facilitating the measurement of reproducible high-resolution molecular images which reflect the expected 4-fold symmetry of the molecule. Recently,

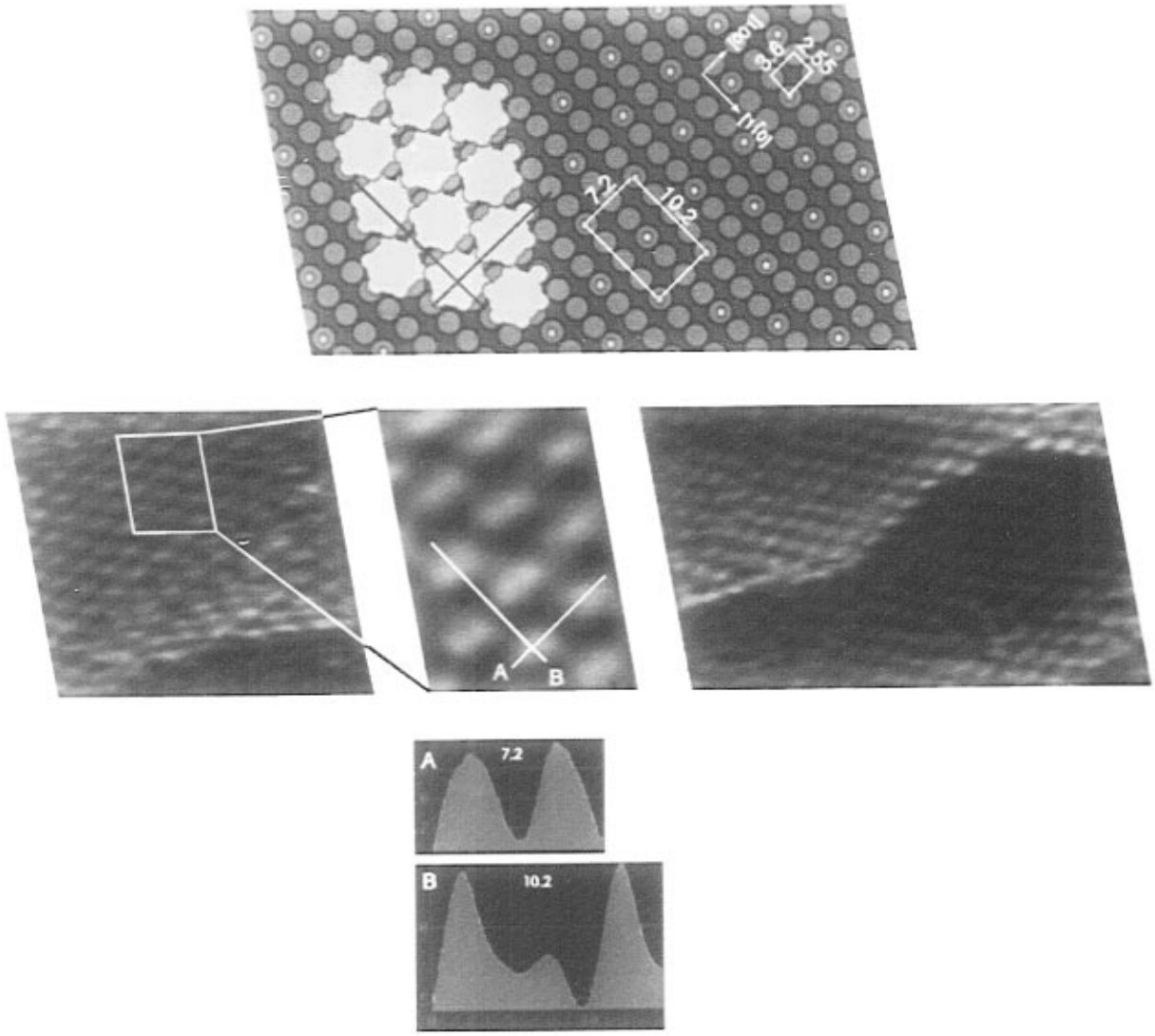

Figure 7. STM topographic image and proposed structure for c(4×2) phenoxy overlayer on Cu(110) at 300 K. All numbers are in angstroms. Two cross sections (A and B) are shown with peak-to-peak distances corresponding to the unit cell of the c(4×2) structure indicated in the structural model. The corrugation heights are 0.7−0.9 Å: $V_{sample} = -94.2$ mV, $I_t = 1.09$ nA. (Reprinted from ref 67. Copyright 1995 Elsevier.)

these images were more carefully interpreted using the ESQC theoretical technique.[50]

High-resolution images have also been obtained for Cu-phth on the following substrates: GaAs(110),[72] Si-(100) (2×1),[73] Si(100) and Si(111),[74] reduced $SrTiO_3$,[75] and HOPG and MoS_2.[76] For all of these systems, the molecular images have 4-fold symmetry, typically appearing like a clover leaf, reflecting the shape of the Cu-phth molecule.

b. Other Porphyrins

Lead phthalocyanine (Pb-phth) has also been successfully imaged on MoS_2.[77] Unlike Cu-phth, this molecule is nonplanar due to the large ion radius of the Pb^{2+}. The molecule can appear in two different states in submolecularly resolved clover-leaf-type images, with either a dark or bright center, an effect attributed to the two possible adsorption geometries, with the molecule adsorbed with the Pb above or below the molecular plane. Transitions between the two states were observed and could also be explicitly induced by applying voltage pulses with the tunneling tip. The crystallographic structure of the Pb-phth layers was determined with respect to the underlying substrate structure by comparing images of the overlayer with those of the substrate. The substrate was imaged by increasing the tunneling current to several nanoamperes so that the molecules were removed by the tip, leaving the underlying substrate visible. Three different crystallographic phases in the arrangement of the Pb-phth on the surface were identified: a close-packed phase, a rowlike phase, and a phase in which three close-packed rows alternate with one or two isolated single rows.

The molecule copper tetra(3,5-di-*tert*-butylphenyl)-porphyrin (Cu-TBP-porphyrin) with four di-*tert*-butylphenyl (DTP) substituents (legs) has also been imaged with very high resolution on Cu(100).[78] The image of each molecule consists of four bright spots, corresponding to the four DTP substituents (Figure 9). This particular molecule−substrate system allowed the achievement of two-dimensional positioning of intact individual molecules at room temperature using an STM tip to "push" the molecules across the surface. The DTP groups allowed a strong enough interaction with the surface to prevent ther-

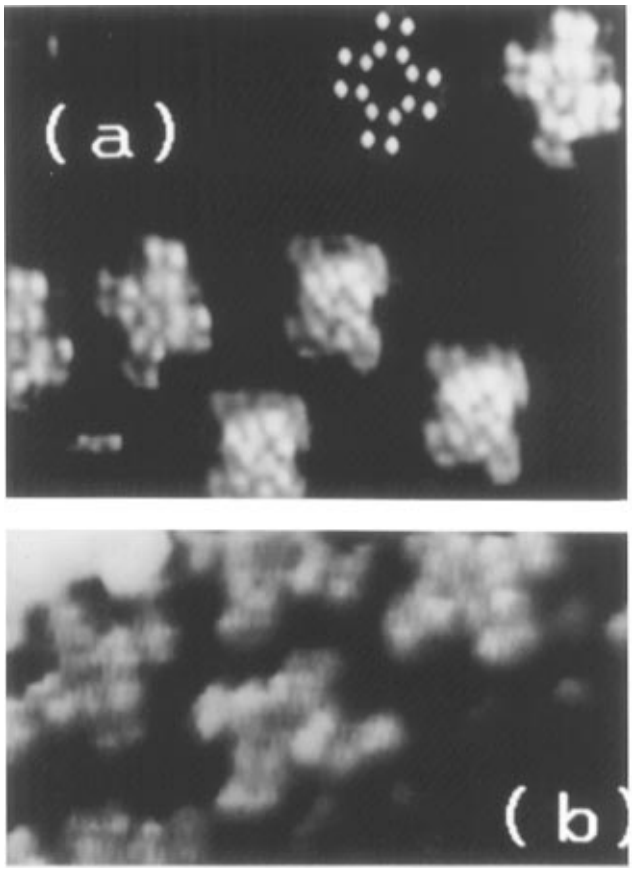

Figure 8. (a) High-resolution image of Cu-phth on Cu(100) at submonolayer coverage: $V_t = -0.15$ V, $I_t = 2$ nA. Molecule corrugation is ~2 Å. A gray scale representation of the HOMO, evaluated at 2 Å above the molecular plane, has been embedded in the image. (b) High-resolution image near 1 ML coverage: $V_t = -0.07$ V, $I_t = 6$ nA. (Reprinted from ref 37. Copyright 1989 American Institute of Physics.)

mally activated molecular diffusion, but also allowed molecular translation with the tunneling tip. Imaging was performed at high gap resistance (27.5 GΩ, with $V_t \approx \pm 2200$ mV, $I_t \approx 80$ pA), and manipulation was at low gap resistance (10−15 MΩ, with $V_t \approx \pm 30$ mV, $I_t \approx 2-3$ nA). Molecular mechanics simulations demonstrated the crucial role of flexure during the positioning process. STM images of the same molecule on Cu(100), Au(110), and Ag(110) have also been used for the first time to give conformational analysis of an individual molecule in real space.[79]

IV. Carbon Monoxide

The first images of individual molecules of adsorbed carbon monoxide were obtained by Eigler and co-workers, using an STM operating at 4 K.[32] CO molecules on Pt(111) appeared in two different forms, a "bump" and a "sombrero." Furthermore, the appearance of a CO molecule could be changed between the two forms by sliding it along the surface. From the stability of the structures, the number of possible sites for a particular form per unit cell, and consistency with other surface science measurements such as infrared and electron energy loss spectroscopies and LEED, the bump state was assigned to CO bonded in an on-top site and the sombrero state to a bridge site. Theoretical calculations of the expected images confirmed these assignments.[80] The theory also allowed detailed understanding of the through-space and through-molecule components of the tunneling current and their effects on the observed STM images.

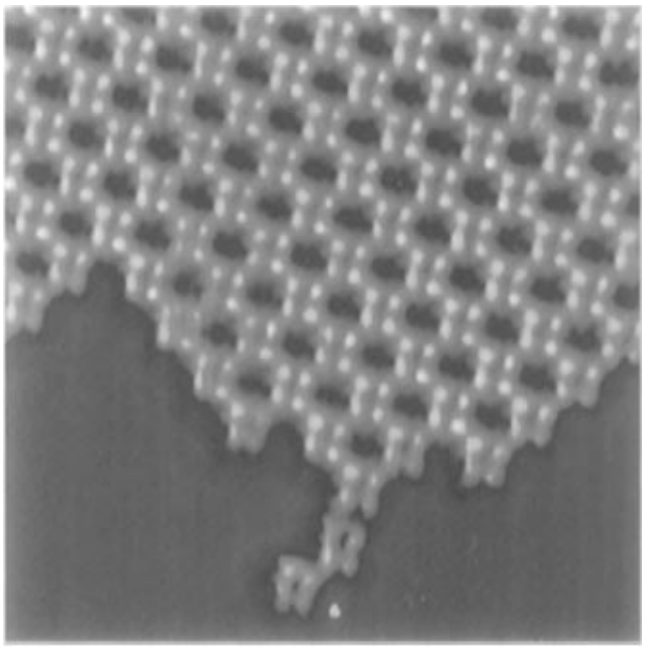

Figure 9. STM topograph of Cu-TBP-porphyrin on Cu(100), showing islands with a $(\sqrt{58}\times\sqrt{58})$ superstructure. Each individual molecule is imaged as four bright lobes corresponding to the four DTP substiutents: $V_t \approx 2200$ mV and $I_t \approx 80$ pA. Image area is 21 nm × 21 nm. (Reprinted from ref 78. Copyright 1996 American Association for the Advancement of Science.)

Meyer, Neu, and Rieder also observed individual carbon monoxide molecules on Cu(211) at low temperatures between 30 and 80 K.[31,81−83] In some images, usually at high CO coverage, the molecules appeared as bumps, while in others, usually for low coverage, they appeared as dips (Figure 10). Thus, a difference in chemical composition of the tip was inferred, with a metallic tip used to produce images with molecules appearing as dips, and a molecule at the tip apex for images in which the molecules appeared as bumps. Several different ordered structures for the CO molecules were identified, including a (2×1) phase corresponding to $^1/_2$ ML coverage, a (3×1) phase with $^2/_3$ ML, and a (4×1) phase with $^3/_4$ ML.[31] The molecular images gave the absolute coverage determinations, as well as the registry of the adsorbates with respect to the substrate. The individual CO molecules were also moved laterally along the surface with the STM tip, and the molecules on the surface were arranged to formed the letters "F" and "U" for the abbreviation of the authors' university.[81−83] The principles for laterally moving atoms and molecules and repositioning them into atomic scale structures were developed by Eigler and co-workers.[32,84,85] To move CO molecules across the surface, the tip is brought close to the molecule by reducing the tunneling resistance to about 1 MΩ, and then the tip is moved parallel to the surface, dragging or pushing the molecule with it. Then, the tip is withdrawn slightly to the scanning mode distance, and a new STM picture is measured to check the result of the manipulation. For CO on Cu(211), the

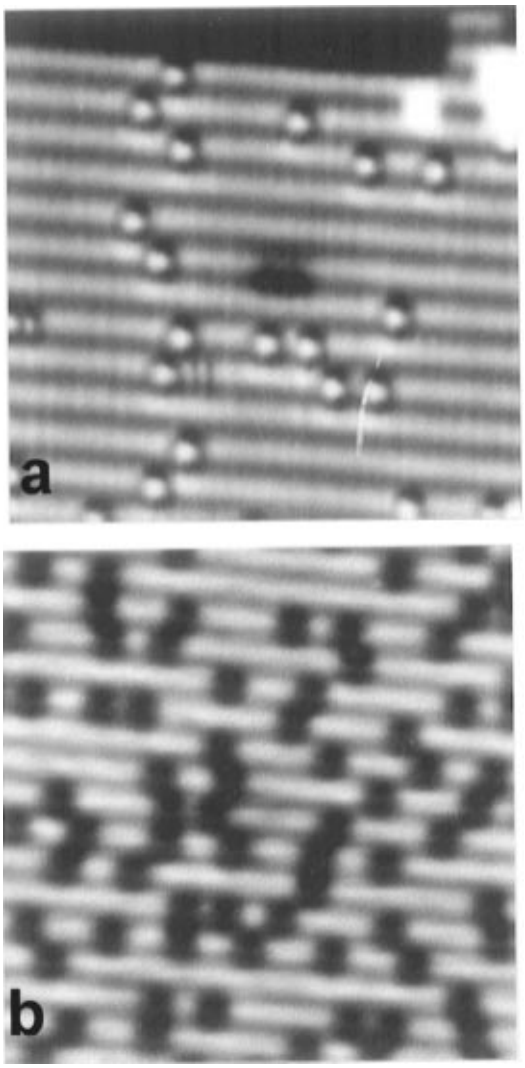

Figure 10. STM images of CO on Cu(211) at low coverage at 30 K. (a) CO molecules appear as bumps 0.2 Å high: 0.05 ML of CO, $V_{sample} = -1.3$ V, 0.1 nA, 8 nm × 8 nm. (b) CO molecules appear as dips: 0.12 ML of CO, $V_{sample} =$ 0.1 V, 0.1 nA, 10 nm × 10 nm. (Reprinted from ref 31. Copyright 1995 Elsevier.)

anisotropy of the substrate results in CO molecules moving easily along the step edges, but motion perpendicular to the steps is difficult.

In contrast with earlier studies reporting that chemisorbed CO could not be atomically resolved at room temperature in STM images,[2,3,86,87] it has now been demonstrated that CO can indeed be imaged at room temperature by STM for several different systems. These include CO adsorbed on Ni(110),[88] Ni(111),[89] and $Pt_{0.1}Ni_{0.9}$(100) alloy.[90] For these systems, the STM images are used to determine the overlayer structure directly, as well as to determine the adsorbate binding site. Atomically resolved STM imaging of CO on Ni(110) and Ni(111) was only possible for a saturated adlayer, achieved under a relatively high pressure of CO gas (10^{-6} mbar), presumably because frustrated molecular vibrations and rotations were minimized under these conditions. The images were used to demonstrate that the Ni(110) (2×1) 2CO structure consists of zigzag rows of CO oriented along the Ni[1$\bar{1}$0] row, alternately tilted away from the normal within the (001) plane[88] (Figure 11). By coadsorbing the molecules with a small amount of O or S, which have known registry with respect to the substrate and the CO overlayer, the CO was shown to be bonded in the short bridge site at saturation coverage. For the Ni(111) c(4×2) 2CO structure at room temperature, the CO was seen to occupy both fcc and hcp 3-fold hollow adsorption sites with the molecular axis tilted with respect to the surface normal.[89] Carbon monoxide adsorbed in a full c(2×2) overlayer on $Pt_{0.1}Ni_{0.9}$(100) lifted the shifted row reconstruction of the substrate.[90] Simultaneous imaging of the molecules with the substrate led to an assignment of the on-top site for the CO.

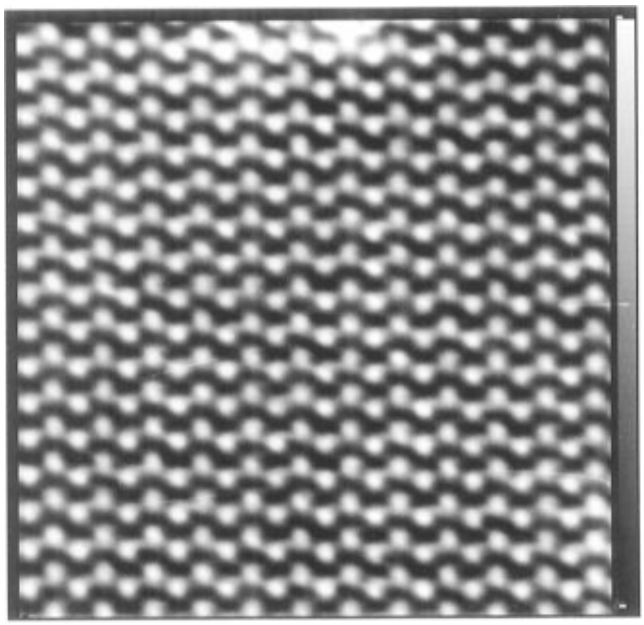

Figure 11. STM image of clean Ni(110) exposed to CO at 10^{-6} mbar pressure at room temperature clearly shows (2×1) structure with 2 molecules per unit cell corresponding to 1 ML of CO coverage (60 Å × 60 Å). (Reprinted from ref 88. Copyright 1995 Elsevier.)

Several studies have involved the coadsorption of CO with other atoms, such as S, O, and K, on metal surfaces. For the CO/O/Ni(110) and CO/S/Ni(110) systems at room temperature, the coadsorbed species phase separate in large domains due to the large local repulsion between the differing species.[91] The addition of CO to precovered O/Ni(110) and S/Ni(110) causes an increase in the ordering of the O (3×1) and S c(2×2) structures respectively. For local coverage of CO less than saturation, individual CO molecules are not resolved. Again, however, when the partial pressure of CO is raised to 10^{-6} mbar, individual CO molecules are resolved in the p2mg(2×1) structure for both systems.

The addition of adsorbed CO onto p(2×2) S on Re(0001) and on Pt(111) results in compression of the sulfur layers into ordered structures of high local coverage.[92,93] A very unique surface reconstruction was observed for coadsorbed CO and S on a stepped (approximately 5° miscut) Pt(111) surface. The two species segregated, and the surface restructured via step splitting, with new metal terraces formed, each containing a different adsorbate.[94] For these three systems, however, the CO molecules were not individually resolved at room temperature, presumably as a result of their rapid diffusion during the imaging. A study of CO adsorbed onto K-precovered Ni-

(100) showed small ordered K−CO islands in STM images, with protrusions arranged in a p(2×2) array ascribed to the K atoms; again, individual CO molecules were not observed.[95]

STM images are now beginning to yield valuable information on the details of chemical reactions. Crew and Madix performed a study in which they used STM images to study the site specificity and reaction kinetics of the oxidation of CO on Cu(110) at 400 K to form carbon dioxide.[96] The catalytic reaction proceeds via a Langmuir−Hinshelwood process, in which the reaction occurs between two adsorbed species:

$$CO(ad) + O(ad) \rightarrow CO_2(g)$$

The STM was used to monitor this ongoing chemical reaction at elevated temperatures. The p(2×1) overlayer of oxygen on Cu(110), consisting of -Cu−O−Cu− "added rows" was clearly observed. In these experiments, the CO reacted with oxygen along the (001) oxygen rows, leaving a clean surface. The adsorbed CO molecules themselves were not observed in the STM images because of their short lifetime (∼1 μs) on the surface and their low equilibrium surface concentration ($<10^{-3}$ ML). Nevertheless, by examining the coverage of oxygen and the shapes of oxygen islands as a function of carbon monoxide exposure and time in subsequent STM images, the reaction appeared to occur initially at the outer edge of an oxygen island, creating kink defects in the overlayer structure. A model was suggested in which adsorbed oxygen, formed by -Cu−O- chain scission at defect sites, is reactive to CO, in contrast to p(2×1) oxygen in the chains, which is not reactive. This model also explains the oxidation of CO on the same substrate at 150 K.[97] In the study at lower temperature, the same authors observed coadsorbed CO and oxygen on Cu(110) at 150 K, and the adsorbed CO appeared as regularly spaced stripes along the (110) direction in the clean surface regions between p(2×1) oxide islands. At the lower temperature, the CO does not react with precovered oxygen on the surface, presumably because of the strong chemisorption of the oxygen. Instead, carbon dioxide is formed when a surface partially covered with p(2×1) oxide and coadsorbed CO is exposed to oxygen.

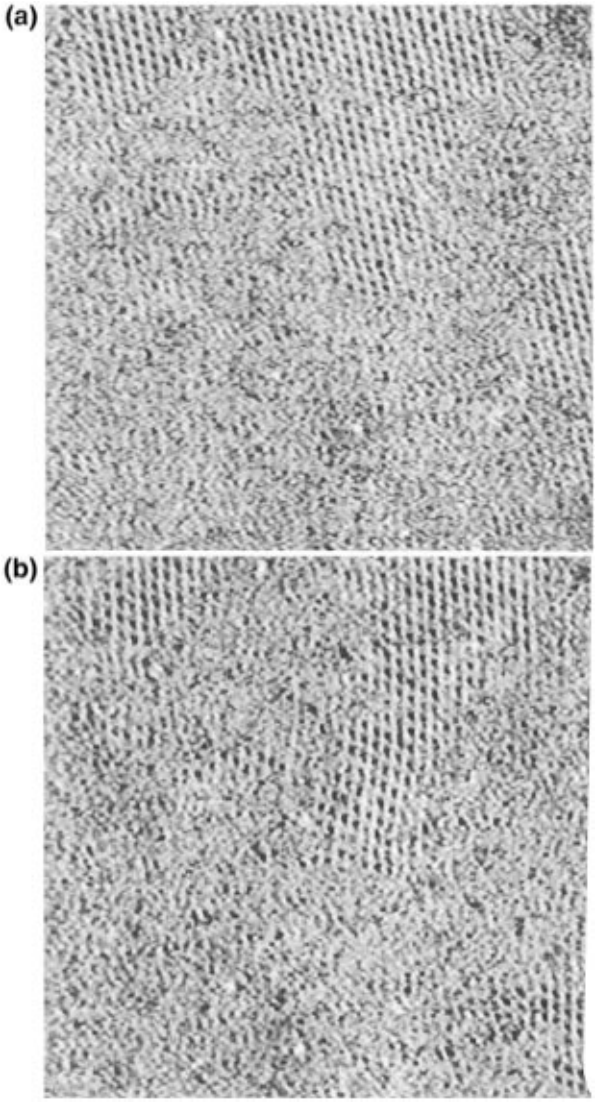

Figure 12. These 400 Å × 400 Å STM images of the chemical reaction of ethylene to ethylidyne on Pt(111) were obtained as a function of time at 230 K. In these images, areas covered by ethylene molecules appear as the well-ordered pattern, and areas covered by ethylidyne molecules appear as a rather disordered pattern. (a) Image obtained after annealing the sample for several minutes at 230 K. (b) Image obtained on the same area of the surface kept for several additional minutes at the same temperature. (Reprinted from ref 99. Copyright 1992 American Institute of Physics.)

V. Ethylene

Land et al. performed one of the first STM studies which follows a chemical reaction as a function of temperature, using the adsorption system of ethylene (C_2H_4) on Pt(111).[98−100] This system has been widely studied by many surface science techniques, and the following reaction steps have been identified.[101−103] Ethylene adsorbs with the C═C bond parallel to the Pt surface for temperatures up to 230 K. For 230 K $< T <$ 450 K, ethylene converts to ethylidyne (CCH_3) on the surface, with ethylidyne bonded with the C−C bond perpendicular to the surface. Between 450 and 770 K, further dehydrogenation of the ethylidyne leads to the formation of "carbidic" carbon on the surface. Above 800 K, the carbon converts to a graphitic structure. STM images in a variable temperature instrument were used by Land et al. to observe all of the steps in the reaction series.

For ethylene on Pt(111) at 160 K, the STM images show an ordered pattern of structures of the size of ethylene molecules.[98] Annealing to 350 K leads to the formation of ethylidyne on the surface, but the STM sees no discernible molecular structures. When the annealed surface was cooled to 180 K, however, the STM images show both ethylene, which has long-range order and a sharper pattern, and ethylidyne, which appears rather disordered with a fuzzier pattern.[99] The lower temperature presumably reduces the molecular motion, allowing the STM to resolve individual molecules. In situ STM imaging of the conversion of ethylene to ethylidyne at 230 K as a function of time was performed.[99] Figure 12 shows two images obtained during the reaction

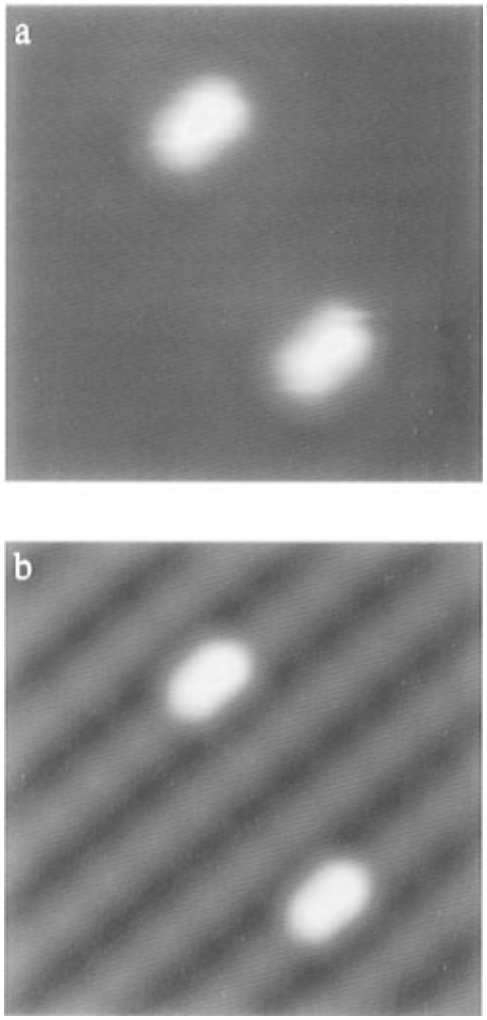

Figure 13. (a) Unprocessed data and (b) processed (Fourier filtered) data of two ethylene molecules on a Cu(110) surface: field of view 20 Å × 20 Å, molecular height ~1.5 Å, $V_t = -20$ meV, $I_t = 50$ pA. (Reprinted from ref 106. Copyright 1997 Royal Society of Chemistry.)

process. Figure 12a corresponds to a partially-reacted surface, after the sample has been held at 230 K for several minutes, while Figure 12b was recorded several minutes later. Some small white protrusions can be used as markers to compare the figures. The well-ordered sharper structures in the top center, upper left, and middle right edge of Figure 12a correspond to ethylene, while the fuzzy, less-ordered structures in the rest of the images correspond to ethylidyne. The reaction appears to occur at the edges of the ethylene islands. This mesoscopic behavior observed in the STM images is directly related to the macroscopic kinetics of the reaction, which were recently shown to exhibit non-first-order behavior in laser-induced thermal desorption Fourier transform mass spectrometry experiments by Erley et al.[104] Computer simulations showed that this behavior is consistent with the STM observations of a reaction dominated by island boundaries. These experiments were directly stimulated by the STM observations and show how high-resolution images can contribute to the development of a detailed understanding of macroscopic phenomena.

Further heating of the ethylidyne covered Pt(111) surface above 430 K results in further dehydrogenation, leaving carbonaceous particles on the surface which are observed in the STM images.[99] Annealing to high temperatures and then imaging at room temperature, the following structures are seen: 700 K, carbonaceous particles 10−15 Å in diameter uniformly distributed across the surface; 800 K, graphite islands 20−30 Å in diameter uniformly distributed across the surface; 1070 K, graphite islands accumulating at lower step edges, together with many small islands on the terraces; 1230 K, larger graphite islands at step edges and fewer large, regularly shaped islands on the terraces.[100]

Individual molecules of ethylene on Cu(110) have recently been observed in an STM operating at 4 K.[105,106] Figure 13 shows (a) unprocessed and (b) processed (Fourier filtered) data. The processed data show clearly the molecule and the corrugation of the underlying metal lattice. It is clear that the ethylene molecule is adsorbed on the close-packed rows, with the C−C axis parallel to the surface and oriented in the ⟨110⟩ direction. Although the molecule appears in the processed image to occupy the short bridge binding site on the close-packed rows, more recent data suggests that it may not be possible to distinguish between the short bridge and atop sites.

VI. Other Molecules

STM imaging has also been used to study deposition of methanol on Cu(110) and the steps in the synthesis of formaldehyde.[107] Methanol deposited onto oxygen-predosed Cu(110) gives a methoxy species, which then forms formaldehyde upon heating to 300 K.

$$2CH_3OH(ad) + O(ad) \rightarrow 2CH_3O(ad) + H_2O(g)$$

$$2CH_3O(ad) \rightarrow 2CH_2O(g) + H_2(g)$$

Upon dosing the (2×1)O/Cu(110) added row reconstruction at 270 K with 10 L of methanol, the surface appears to be covered by "zigzag" chainlike structures in the [001] direction, separated by c(2×2) areas[107] (Figure 14). The (2×1) O islands are seen to react away anisotropically in subsequent images, being replaced by zigzag chains and c(2×2) subunits of the methoxy. The conversion from methanol to methoxy appears to occur via the removal of oxygen from the ends of the (2×1) O islands. When the sample warmed to room temperature, the methoxy islands disappeared, presumably one of the steps in the synthesis of formaldehyde. Smaller methoxy islands disappeared first, and these islands shrink in the [001] direction, releasing incorporated Cu atoms.

Formic acid, benzoic acid, and acetic acid have also been deposited on Cu(110), and the resulting surface-bound formate, benzoate, and acetate species have been imaged by STM.[108−110] Formic acid deposited onto <0.25 ML of O/Cu(110) results in formate on the surface in a c(2×2) structure, while for higher O coverage, the two adsorbates mainly phase separate into islands of c(6×2) oxygen and (3×1) formate.[109] Adsorbed formate and benzoate species on Cu(110) cause step faceting, with bunched equidistant steps aligned along the ⟨112⟩ directions.[108] LEED and STM show that adsorbed acetate, presumably standing vertically on the surface, forms highly ordered

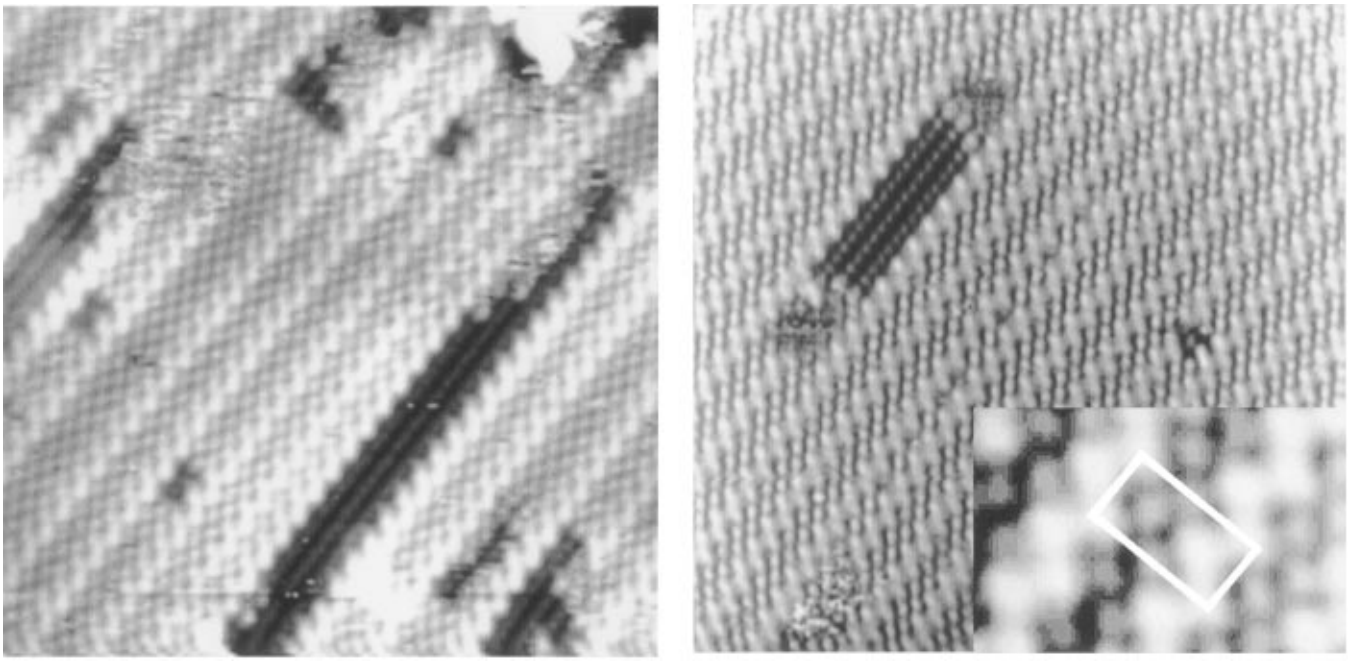

Figure 14. Areas (200 Å × 200 Å) of Cu(110) surface. (a, left) With 5 L of oxygen, followed by cooling and dosing with 10 L of methanol, image shows (2×1) O areas coexisting with methoxy-induced "zigzag" chain and c(2×2) structures. (b, right) Similar area as a after 40 min. Amount of (2×1) area has been reduced, and surface has evolved into (5×2) reconstruction. A (5×2) unit cell is outlined within the inset in b. (Reprinted from ref 107. Copyright 1994 American Institute of Physics.)

$\begin{pmatrix} -1 & 1 \\ 4 & 4 \end{pmatrix}$ and $\begin{pmatrix} 1 & 1 \\ 4 & -4 \end{pmatrix}$ domains, indicative of long-range interactions.[110] Observation of step edge structures gives evidence that the molecular adsorption leads to restructuring of the metal surfaces.

In STM images of 1,3-butanediol adsorbed on Ag(111), the molecule appears as a depression, each of which is considerably larger than the size of a single molecule.[111] The sample bias, varied between −1.5 and +1.5 V, affects the width of the depressions more than their depth. The anomalous appearance of the molecule is attributed to a screening effect, in which the adsorbate reduces the metallic density of states near the Fermi level, in a manner similar to that predicted by Lang for He atoms adsorbed on a metal surface.[112]

STM studies have been performed for ammonia deposited onto O-covered Rh(110)[113] and O-covered Cu(110).[114] The ammonia dehydrogenates for both of these systems leaving surface-bound N. Similarly, an STM study has been performed on NO dissociating on Cu(100) to form adsorbed O and N.[115] These three studies provide additional examples of how the STM can be used to follow chemical reactions.

VII. Conclusions

Clearly, significant progress has been made in using the STM to image individual small molecules on metal surfaces in UHV in the last few years. Many different molecules have been successfully imaged under a variety of conditions: low and room temperature, physisorbed and chemisorbed, low and saturated coverage, varied tunneling voltage and current parameters, and coadsorbed with other atoms and molecules. These molecules have included aromatics, porphyrins, CO, ethylene, and other species. On several systems, the STM has been used to elucidate the details of chemical reactions on an atomic scale in real space, including reactivity at steps and defects. The combination of theory and experiment allows the identification of different types of molecules on a surface. Molecular binding sites, orientations, diffusion rates, and sticking coefficients can all be inferred from STM images. Further progress will undoubtedly be made in the near future in using the real space imaging capabilities of the STM to better understand both details of the adsorption of molecules and the elucidation of more complicated chemical reactions on surfaces.

VIII. Acknowledgments

The author thanks her former colleagues at IBM for their help with some of the molecular studies described here: V. M. Hallmark, R. J. Wilson, P. H. Lippel, H. Ohtani, and C. M. Mate. She thanks V. M. Hallmark and G. W. Anderson for helpful discussions during the writing of this manuscript. She also thanks the National Science Foundation (grant no. CHE-95-20366) and the Campus Laboratory Collaboration Program of the University of California Office of the President for supporting her current research on STM imaging of molecules.

IX. References

(1) Binnig, G.; Rohrer, H.; Gerber, Ch.; Weibel, E. *Phys. Rev. Lett.* **1982**, *49*, 57−61.
(2) Behm, R. J.; Hosler, W.; Ritter, E.; Binnig, G. *Phys. Rev. Lett.* **1986**, *56*, 228−231.
(3) Ritter, E.; Behm, R. J.; Potsche, G.; Wintterlin, J. *Surf. Sci.* **1987**, *181*, 403−411.
(4) Gimzewski, J. K.; Stoll, E.; Schlittler, R. R. *Surf. Sci.* **1987**, *181*, 267−277.
(5) Smith, D. P. E.; Bryant, A.; Quate, C. F.; Rabe, J. P.; Gerber, Ch.; Swalen, J. D. *Proc. Natl. Acad. Sci. U.S.A.* **1987**, *84*, 969.
(6) Wolkow, R.; Avouris, Ph. *Phys. Rev. Lett.* **1988**, *60*, 1049−1052.
(7) Chiang, S. In *Scanning Tunneling Microscopy I*, 2nd ed.; Güntherodt, H.-J., Wiesendanger, R., Eds.; Springer-Verlag: Berlin, 1994; pp 181−205, 258−267.

(8) Sleator, T.; Tycko, R. *Phys. Rev. Lett.* **1988**, *60*, 1418−1421.
(9) Foster, J. S.; Frommer, J. E. *Nature* **1988**, *333*, 542−545.
(10) Foster, J. S.; Frommer, J. E.; Spong, J. K. *Proc. SPIE* **1989**, *1080*, 200−208.
(11) Smith, D. P. E.; Hörber, H.; Gerber, Ch.; Binnig, G. *Science* **1989**, *245*, 43−45.
(12) Hara, M.; Iwakabe, U.; Tochigi, K.; Sasabe, H.; Garito, A. F.; Yamada, A. *Nature* **1990**, *344*, 228−230.
(13) Albrecht, T. R.; Dovek, M. M.; Lang, C. A.; Grütter, P.; Quate, C. F.; Kuan, S. W. J.; Frank, C. W.; Pease, R. F. W. *J. Appl. Phys.* **1988**, *64*, 1178−1184.
(14) Dovek, M. M.; Albrecht, T. R.; Kuan, S. W. J.; Lang, C. A.; Emch, R.; Grütter, P.; Frank, C. W.; Pease, R. F. W.; Quate, C. F. *J. Microsc.* **1988**, *152*, 229−236.
(15) Piner, R.; Reinfenberger, R.; Martin, D. C.; Thomas, E. L.; Apkarian, R. P. *J. Polym. Sci., Part C: Polym. Lett.* **1990**, *28*, 399.
(16) Reneker, D. H.; Schneir, J.; Howell, B.; Harary, H. *Polym. Commun.* **1990**, *31*, 167.
(17) Wilson, R. J.; Meijer, G.; Bethune, D. S.; Johnson, R. D.; Chambliss, D. D.; deVries, M. S.; Hunziker, H. E.; Wendt, H. R. *Nature* **1990**, *348*, 621−622.
(18) Altman, E. I.; Colton, R. J. *Phys. Rev. B* **1993**, *48*, 18244−18249.
(19) Hasizume, T.; Motai, K.; Wang, X. D.; Sinohara, H.; Saito, Y.; Maruyama, Y.; Ohno, K.; Kawazoe, Y.; Nishina, Y.; Pickering, H. W.; Kuk, Y.; Sakurai, T. *Phys. Rev. Lett.* **1993**, *71*, 2959−2962.
(20) Kuk, Y.; Kim, D. K.; Suh, Y. D.; Park, K. H.; Noh, H. P.; Ohn, S. J.; Kim, S. K. *Phys. Rev. Lett.* **1993**, *70*, 1948−1951.
(21) Li, Y. Z.; Patrin, J. C.; Chander, M.; Weaver, J. H.; Chibante, L. P. F.; Smalley, R. E. *Science* **1991**, *252*, 547−551.
(22) Xu, H.; Chen, D. M.; Creager, W. N. *Phys. Rev. Lett.* **1993**, *70*, 1850−1853.
(23) Gaisch, R.; Berndt, R.; Gimzewski, J. K.; Reihl, B.; Schlittler, R. R.; Schneider, W. D.; Tschudy, M. *Appl. Phys. A* **1993**, *57*, 207−210.
(24) Wang, X.-D.; Hashizume, T.; Sakurai, T. *Mod. Phys. Lett. B* **1994**, *8*, 1597−1626.
(25) Yao, X.; Ruskell, T. G.; Workman, R. K.; Sarid, D.; Chen, D. *Surf. Sci.* **1996**, *367*, L85−L90.
(26) Guckenberger, R.; Hartmann, T.; Wiegräbe, W.; Baumeister, W. In *Scanning Tunneling Microscopy II*; Güntherodt, H.-J., Wiesendanger, R., Eds.; Springer-Verlag: Berlin, 1992; pp 51−97.
(27) Ramos, M. M. D. *J. Phys.: Condens. Matter* **1993**, *5*, 2843−2848.
(28) Nawaz, Z.; Cataldi, T. R. I.; Knall, J.; Somekh, R.; Pethica, J. B. *Surf. Sci.* **1992**, *265*, 139−155.
(29) Richter, S.; Manassen, Y. *J. Phys. Chem.* **1994**, *98*, 2941−2949.
(30) Hörber, J. K. H.; Häberle, W.; Ruppersberg, P.; Niksch, M.; Smith, D. P. E.; Binnig, G. *J. Vac. Sci. Technol. B* **1994**, *12*, 2243−2246.
(31) Meyer, G.; Neu, B.; Rieder, K. H. *Chem. Phys. Lett.* **1995**, *240*, 379−384.
(32) Stroscio, J. A.; Eigler, D. M. *Science* **1991**, *254*, 1319−1326.
(33) Avouris, Ph. *Acc. Chem. Res.* **1995**, *28*, 95−102.
(34) Chiang, S.; Hallmark, V. M.; Meinhardt, K.-P.; Hafner, K. *J. Vac. Sci. Technol. B* **1994**, *12*, 1957−1962.
(35) Hallmark, V. M.; Chiang, S. *Surf. Sci.* **1993**, *286*, 190−200.
(36) Sautet, P.; Bocquet, M.-L. *Phys. Rev. B* **1996**, *53*, 4910−4925.
(37) Lippel, P. H.; Wilson, R. J.; Miller, M. D.; Wöll, Ch.; Chiang, S. *Phys. Rev. Lett.* **1989**, *62*, 171−174.
(38) Spong, J. K.; Mizes, H. A.; LaComb, L. J., Jr.; Dovek, M. M.; Frommer, J. E.; Foster, J. S. *Nature* **1989**, *338*, 137−139.
(39) Garcia, R.; Garcia, N. *Chem. Phys. Lett.* **1990**, *173*, 44−50.
(40) Hörber, J. K. H.; Lang, C. A.; Hänsch, T. W.; Heckl, W. M.; Möhwald, H. *Chem. Phys. Lett.* **1988**, *145*, 151−158.
(41) Joachim, C.; Sautet, P. In *Scanning Tunneling Microscopy and Related Methods*; Behm, R. J., Garcia, N., Rohrer, H., Eds.; Kluwer: The Netherlands, 1989; p 377.
(42) Amrein, M.; Stasiak, A.; Dürr, R.; Gross, H.; Travaglini, G. *Science* **1989**, *243*, 1708−1711.
(43) Ohtani, H.; Wilson, R. J.; Chiang, S.; Mate, C. M. *Phys. Rev. Lett.* **1988**, *60*, 2398−2401.
(44) Lin, R. F.; Blackmann, G. S.; Van Hove, M. A.; Somorjai, G. A. *Acta Crystallogr. B* **1987**, *43*, 368−376.
(45) Chiang, S.; Wilson, R. J.; Mate, C. M.; Ohtani, H. *J. Microsc.* **1988**, *152*, 567−571.
(46) Chiang, S.; Wilson, R. J.; Mate, C. M.; Ohtani, H. *Vacuum* **1990**, *41*, 118−120.
(47) Yoon, H. A.; Salmeron, M.; Somorjai, G. A. *Surf. Sci.* **1997**, *373*, 300−306.
(48) Weiss, P. S.; Eigler, D. M. *Phys. Rev. Lett.* **1993**, *71*, 3139−3142.
(49) Sautet, P.; Joachim, C. *Chem. Phys. Lett.* **1991**, *185*, 23−30.
(50) Sautet, P.; Joachim, C. *Surf. Sci.* **1992**, *271*, 387−394.
(51) Stranick, S. J.; Kamna, M. M.; Weiss, P. S. *Science* **1994**, *226*, 99−102.
(52) Stranick, S. J.; Kamna, M. M.; Weiss, P. S. *Surf. Sci.* **1995**, *338*, 41−59.
(53) Yoshinobu, J.; Tanaka, H.; Kawai, T.; Kawai, M. *Phys. Rev. B* **1996**, *53*, 7492−7495.
(54) Stensgaard, I.; Ruan, L.; Lægsgaard, E.; Besenbacher, F. *Surf. Sci.* **1995**, *337*, 190−197.
(55) Strohmaier, R.; Ludwig, C.; Petersen, J.; Gompf, B.; Eisenmenger, W. *Surf. Sci.* **1994**, *318*, L1181−L1185.
(56) Fisher, A. J.; Blöchl, P. E. *Phys. Rev. Lett.* **1993**, *70*, 3263−3266.
(57) Hallmark, V. M.; Chiang, S.; Brown, J. K.; Wöll, Ch. *Phys. Rev. Lett.* **1991**, *66*, 48−51.
(58) Hallmark, V. M.; Chiang, S.; Wöll, Ch. *J. Vac. Sci. Technol. B* **1991**, *9*, 1111−1114.
(59) Chiang, S.; Chambliss, D. D.; Hallmark, V. M.; Wilson, R. J.; Wöll, Ch. In *The Structure of Surfaces III*; Tong, S. Y., Van Hove, M. A., Xide, X., Takayanagi, K., Eds.; Springer-Verlag: Berlin, 1991; pp 204−213.
(60) Hallmark, V. M.; Chiang, S.; Brown, J. K.; Wöll, Ch. In *Synthetic Microstructures in Biological Research*; Schnuir, J. M., Peckerau, M., Eds.; Plenum Press: New York, 1992; pp 79−90.
(61) Hallmark, V. M.; Chiang, S.; Meinhardt, K.-P.; Hafner, K. *Phys. Rev. Lett.* **1993**, *70*, 3740−3743.
(62) Hallmark, V. M.; Chiang, S. *Surf. Sci.* **1995**, *329*, 255−268.
(63) Dahlgren, D.; Hemminger, J. C. *Surf. Sci.* **1981**, *109*, L513−L518; **1982**, *114*, 459.
(64) Frank, E. R.; Chen, X. X.; Hamers, R. J. *Surf. Sci.* **1995**, *334*, L709−L714.
(65) Chen, X.; Frank, E. R.; Hamers, R. J. *J. Vac. Sci. Technol. B* **1996**, *14*, 1136−1140.
(66) Frederick, B. G.; Chen, Q.; Barlow, S. M.; Condon, N. G.; Leibsle, F. M.; Richardson, N. V. *Surf. Sci.* **1996**, *352−354*, 238−247.
(67) Guo, X.-C.; Madix, R. J. *Surf. Sci.* **1995**, *341*, L1065−L1071.
(68) Kim, J.-T.; Kawai, T.; Yoshinobu, J.; Kawai, M. *Surf. Sci.* **1996**, *360*, 50−54.
(69) Strohmaier, R.; Ludwig, C.; Petersen, J.; Gompf, B.; Eisenmenger, W. *Surf. Sci.* **1996**, *351*, 292−302.
(70) Ludwig, C.; Gompf, B.; Petersen, J.; Strohmaier, R.; Eisenmenger, W. *Z. Phys. B: Condens. Matter* **1994**, *93*, 365−373.
(71) Buchholz, J. C.; Somorjai, G. A. *J. Chem. Phys.* **1977**, *66*, 573−580.
(72) Möller, R.; Coenen, R.; Esslinger, A.; Koslowski, B. *J. Vac. Sci. Technol. A* **1990**, *8*, 659−660.
(73) Maeda, Y.; Matsumuto, T.; Kasaya, M.; Kawai, T. *Jpn. J. Appl. Phys. Part 2* **1996**, *35* L405−L407.
(74) Kanai, M.; Kawai, T.; Motai, K.; Wang, X. D.; Hashizume, T.; Sakurai, T. *Surf. Sci.* **1995**, *329*, L619−L623.
(75) Tanaka, H.; Kawai, T. *Jpn. J. Appl. Phys. Part 1* **1996**, *35*, 3759−3763.
(76) Ludwig, C.; Strohmaier, R.; Peterson, J.; Gompf, B.; Eisenmenger, W. *J. Vac. Sci. Technol. B* **1994**, *12*, 1963−1966.
(77) Strohmaier, R.; Ludwig, C.; Petersen, J.; Gompf, B.; Eisenmenger, W. *J. Vac. Sci. Technol. B* **1996**, *14*, 1079−1082.
(78) Jung, T. A.; Schlittler, R. R.; Gimzewski, J. K.; Tang, H.; Joachim, C. *Science* **1996**, *271*, 181−184.
(79) Jung, T. A.; Schlittler, R. R.; Gimzewski, J. K. Preprint.
(80) Bocquet, M.-L.; Sautet, P. *Surf. Sci.* **1996**, *360*, 128−136.
(81) Meyer, G.; Neu, B.; Rieder, K. H. *Appl. Phys. A* **1995**, *60*, 343−345.
(82) Neu, B.; Meyer, G.; Rieder, K. H. *Mod. Phys. Lett.* **1995**, *9*, 963−969.
(83) Meyer, G.; Neu, B.; Rieder, K. H. *Phys. Status Solidi B* **1995**, *192*, 313−324.
(84) Eigler, D. M.; Schweizer, E. K. *Nature* **1990**, *344*, 524−526.
(85) Zeppenfeld, P.; Lutz, C. P.; Eigler, D. M. *Ultramicroscopy* **1992**, *42−44*, 128−133.
(86) Gritsch, T.; Coulman, D.; Behm, R. J.; Ertl, G. *Phys. Rev. Lett.* **1989**, *63*, 1086−1089.
(87) Ramos, M. M. D.; Stoneham, A. M.; Sutton, A. P.; Pethica, J. B. *J. Phys.: Condens. Matter* **1990**, *2*, 5913−5917.
(88) Sprunger, P.; Besenbacher, F.; Stensgaard, I. *Surf. Sci.* **1995**, *324*, L321−L327.
(89) Sprunger, P.; Besenbacher, F.; Stensgaard, I. *Chem. Phys. Lett.* **1995**, *243*, 439−444.
(90) Schmid, M.; Biedermann, A.; Böhmig, S. D.; Weigand, P.; Varga, P. *Surf. Sci.* **1994**, *318*, 289−298.
(91) Sprunger, P.; Besenbacher, F.; Stensgaard, I.; Lægsgaard, E. *Surf. Sci.* **1994**, *320*, 271−280.
(92) Dunphy, J. C.; McIntyre, B. J.; Gomez, J.; Ogletree, D. F.; Somorjai, G. A.; Salmeron, M. B. *J. Chem. Phys.* **1994**, *100*, 6092−6097.
(93) McIntyre, B. J.; Salmeron, M.; Somorjai, G. A. *Surf. Sci.* **1995**, *323*, 189−197.
(94) Batteas, J. D.; Dunphy, J. C.; Somorjai, G. A.; Salmeron, M. *Phys. Rev. Lett.* **1996**, *77*, 534−537.
(95) Murray, S. J.; Finetti, P.; Leibsle, F. M.; Diehl, R. D.; McGrath, R. *Chem. Phys. Lett.* **1995**, *237*, 474−479.
(96) Crew, W. W.; Madix, R. J. *Surf. Sci.* **1996**, *349*, 275−293.
(97) Crew, W W.; Madix, R. J. *Surf. Sci.* **1996**, *356*, 1−18.
(98) Land, T. A.; Michely, T.; Behm, R. J.; Hemminger, J. C.; Comsa, G. *Appl. Phys. A* **1991**, *53*, 414−417.
(99) Land, T. A.; Michely, T.; Behm, R. J.; Hemminger, J. C.; Comsa, G. *J. Chem. Phys.* **1992**, *97*, 6774−6783.
(100) Land, T. A.; Michely, T.; Behm, R. J.; Hemminger, J. C.; Comsa, G. *Surf. Sci.* **1992**, *264*, 261−270.

(101) Koestner, R. J.; Stöhr, S.; Gland, J. L.; Hosley, J. A. *Chem. Phys. Lett.* **1984**, *105*, 332−335.
(102) Steininger, H.; Ibach, H.; Lehwald, S. *Surf. Sci.* **1982**, *117*, 685−698.
(103) Pettiete-Hall, C. L.; Land, D. P.; McIver, R. T.; Hemminger, J. S. *J. Phys. Chem.* **1990**, *94*, 1948.
(104) Erley, W.; Li, Y.; Land, D. P.; Hemminger, J. C. *Surf. Sci.* **1994**, *301*, 177−196.
(105) Buisset, J.; Rust, H.-P.; Schweizer, E. K.; Cramer, L.; Bradshaw, A. M. *Phys. Rev. B* **1996**, *54*, 10373−10376.
(106) Doering, M.; Buisset, J.; Rust, H.-P.; Briner, B. G.; Bradshaw, A. M. *Discuss. Faraday Soc.* **1997**. In press.
(107) Leibsle, F. M.; Francis, S. M.; Davis, R.; Xiang, N.; Haq, S.; Bowker, M. *Phys. Rev. Lett.* **1994**, *72*, 2569−2572.
(108) Leibsle, F. M.; Haq, S.; Frederick, B. G.; Bowker, M.; Richardson, N. V. *Surf. Sci.* **1995**, *343*, L1175−L1181.
(109) Bowker, M.; Rowbotham, E.; Leibsle, F. M.; Haq, S. *Surf. Sci.* **1996**, *349*, 97−110.
(110) Haq, S.; Leibsle, F. M. *Surf. Sci.* **1996**, *355*, L345−L349.
(111) Chen, X. X.; Frank, E. R.; Hamers, R. J. *J. Vac. Sci. Technol. A* **1994**, *12*, 2091−2096.
(112) Lang, N. D. *Phys. Rev. Lett.* **1986**, *56*, 1164−1167.
(113) Kiskinova, M.; Baraldi, A.; Rosei, R.; Dhanak, V. R.; Thornton, G.; Leibsle, F.; Bowker, M. *Phys. Rev. B* **1995**, *52*, 1532−1535.
(114) Guo, X.-C.; Madix, R. J. *Surf. Sci.* **1996**, *367*, L95−L101.
(115) Dhesi, S. S.; Haq, S.; Barrett, S. D.; Leibsle, F. M. *Surf. Sci.* **1996**, *365*, 602−613.

CR940555A